

Co-existing nonlinear attractors of convective spherical dynamos

Radostin D Simitev^{1,3} and Friedrich H Busse^{2,3}

¹ School of Mathematics and Statistics, University of Glasgow – Glasgow G12 8QW, UK, EU

² Institute of Physics, University of Bayreuth – Bayreuth D-95440, Germany, EU

³ NORDITA, AlbaNova University Center – Stockholm SE-10691, Sweden, EU

E-mail: Radostin.Simitev@glasgow.ac.uk

Abstract

We present new results on the existence of two essentially different chaotic attractors arising in a model of nonlinear convection-driven dynamo process in rotating spherical shells. We establish the existence of a hysteresis loop in the transition between these attractors with variation of the rotation parameter τ . We investigate the width of the basins of attraction of the two distinguishable dynamo states and the possibility of spontaneous transition between them. We propose a possible mechanism for the occurrence of geomagnetic field polarity reversals.

1. Introduction

Recently Simitev and Busse [?] have demonstrated the possibility for the existence of essentially different chaotic dynamo solutions at identical parameter values in an established model of convection-driven dynamos in rotating spherical shells. Their study leaves open a number of important questions some of which we try to address here.

2. Formulation and methods

We consider a spherical fluid shell of thickness d rotating with a constant angular velocity Ω . The existence of a static state is assumed with a temperature distribution $T_S = T_0 - \beta d^2 r^2 / 2$ and a gravity field in the form $\mathbf{g} = -d\gamma \mathbf{r}$, where rd is the length of the position vector with respect to the center of the sphere. This form of temperature profile alludes to the possibility that at least a fraction of the energy available to planetary dynamos is due to radiogenic heat release. In addition to d , we use the time d^2/ν , the temperature $\nu^2/\gamma\alpha d^4$ and the magnetic flux density $\nu(\mu\varrho)^{1/2}/d$ as scales for the dimensionless description of the problem where ν denotes the kinematic viscosity of the fluid, κ its thermal diffusivity, ϱ its density and μ its magnetic permeability. In common with most other simulations of Earth and planetary dynamos [1, 2], we assume the Boussinesq approximation implying a constant density ϱ except in the gravity term where its temperature dependence is taken into account with $\alpha \equiv -(d\varrho/dT)/\varrho = \text{const}$. The equations of motion for the velocity vector \mathbf{u} , the heat equation for the deviation Θ from the

static temperature distribution, and the equation of induction for the magnetic flux density \mathbf{B} are then given by

$$\nabla \cdot \mathbf{u} = 0, \quad \nabla \cdot \mathbf{B} = 0, \quad (1a)$$

$$(\partial_t + \mathbf{u} \cdot \nabla)\mathbf{u} + \tau \mathbf{k} \times \mathbf{u} = -\nabla\pi + \Theta \mathbf{r} + \nabla^2 \mathbf{u} + \mathbf{B} \cdot \nabla \mathbf{B}, \quad (1b)$$

$$P(\partial_t \Theta + \mathbf{u} \cdot \nabla \Theta) = R \mathbf{r} \cdot \mathbf{u} + \nabla^2 \Theta, \quad (1c)$$

$$\nabla^2 \mathbf{B} = P_m (\partial_t \mathbf{B} + \mathbf{u} \cdot \nabla \mathbf{B} - \mathbf{B} \cdot \nabla \mathbf{u}), \quad (1d)$$

where all gradient terms in the equation of motion have been combined into $\nabla\pi$. The dimensionless parameters in our formulation are the Rayleigh number R , the Coriolis number τ , the Prandtl number P and the magnetic Prandtl number P_m ,

$$R = \frac{\alpha\gamma\beta d^6}{\nu\kappa}, \quad \tau = \frac{2\Omega d^2}{\nu}, \quad P = \frac{\nu}{\kappa}, \quad P_m = \frac{\nu}{\lambda}, \quad (2)$$

where λ is the magnetic diffusivity. Being solenoidal vector fields \mathbf{u} and \mathbf{B} can be represented uniquely in terms of poloidal and toroidal components,

$$\mathbf{u} = \nabla \times (\nabla v \times \mathbf{r}) + \nabla w \times \mathbf{r}, \quad (3a)$$

$$\mathbf{B} = \nabla \times (\nabla h \times \mathbf{r}) + \nabla g \times \mathbf{r}. \quad (3b)$$

We assume fixed temperatures at $r = r_i \equiv 2/3$ and $r = r_o \equiv 5/3$ and stress-free rather than no-slip boundary conditions in order to approach, at least to some extent, the extremely low values of viscosity believed to be appropriate to planetary cores [3],

$$\nu = \partial_{rr}^2 v = \partial_r(w/r) = \Theta = 0. \quad (4)$$

For the magnetic field we assume electrically insulating boundaries at $r = r_i$ and $r = r_o$ such that the poloidal function h

matches the function $h^{(e)}$ which describes the potential fields outside the fluid shell,

$$g = h - h^{(e)} = \partial_r(h - h^{(e)}) = 0 \text{ at } r = r_i, r_o. \quad (5)$$

The radius ratio $r_i/r_o = 0.4$ is slightly larger than that appropriate for the Earth's liquid core. This is a standard formulation of the spherical convection-driven dynamo problem [4, 5, 2] for which an extensive collection of results already exists [6, 7, 8, 9]. The results reported below are not strongly model dependent. In particular, dynamos with stress-free and with no-slip velocity boundary conditions as well as with different modes of energy supply are known to have comparable energy densities and symmetry properties (see fig. 15 of [2]). Furthermore, aiming to retain a general physical perspective, we intentionally use a minimal number of physical parameters including only those of primary importance for stellar and planetary applications.

Equations of motion for the scalar fields v , w , are obtained by taking $\mathbf{r} \cdot \nabla \times \nabla \times$ and $\mathbf{r} \cdot \nabla \times$ of equation (1b) and equations for g and h are obtained by taking $\mathbf{r} \cdot \nabla \times$ and $\mathbf{r} \cdot$ of equation (1d). These equations are solved numerically by a pseudo-spectral method as described in [10] based on expansions of all dependent variables in spherical harmonics for the angular dependences and in Chebychev polynomials for the radial dependence. Typically, calculations are considered decently resolved when the spectral power of kinetic and magnetic energy drops by more than a factor of 100 from the spectral maximum to the cut-off wavelength [11]. A minimum of 41 collocation points in the radial direction and spherical harmonics up to the order 96 have been used in all cases reported here which provides adequate resolution as demonstrated in fig. ?? for two typical dynamo solutions. The dynamo solutions are characterized by their magnetic energy densities,

$$\begin{aligned} \overline{M}_p &= \frac{1}{2} \langle |\nabla \times (\nabla \bar{h} \times \mathbf{r})|^2 \rangle, & \overline{M}_t &= \frac{1}{2} \langle |\nabla \bar{g} \times \mathbf{r}|^2 \rangle, \\ \widetilde{M}_p &= \frac{1}{2} \langle |\nabla \times (\nabla \widetilde{h} \times \mathbf{r})|^2 \rangle, & \widetilde{M}_t &= \frac{1}{2} \langle |\nabla \widetilde{g} \times \mathbf{r}|^2 \rangle, \end{aligned}$$

where $\langle \cdot \rangle$ indicates the average over the fluid shell and \bar{h} refers to the axisymmetric component of h , while \widetilde{h} is defined by $\widetilde{h} = h - \bar{h}$. The corresponding kinetic energy densities \overline{E}_p , \overline{E}_t , \widetilde{E}_p and \widetilde{E}_t are defined analogously with v and w replacing h and g . Other global quantities of interest are the helicity of a vector field \mathbf{A} ,

$$H_{\mathbf{A}} = \langle (\nabla \times \mathbf{A}) \cdot \mathbf{A} \rangle,$$

(kinetic helicity when $\mathbf{u} = \mathbf{A}$, and magnetic helicity when $\mathbf{B} = \mathbf{A}$, respectively [magnetic helicity is equivalent to $H_{\mathbf{B}} = \mathbf{j} \cdot \mathbf{B}$]), and the cross-helicity

$$XH = \langle \mathbf{u} \cdot \mathbf{B} \rangle.$$

3. Coexistence

In [?] we have demonstrated bistability and hysteresis as a function of P , P_m and R . Here we would like to establish

that bistability and hysteresis occur also as a function of the last remaining basic parameter of the model, τ .

Figure 1 introduces dynamo solutions, and illustrates two different attractors in a specific example.

Figure 1: Time series of kinetic, E , and magnetic, M , energy densities and the dominant dipolar and quadrupolar coefficients of the poloidal fields, $H_{1,2}^0$, for two essentially different dynamo solutions obtained at identical parameter values. Cases: p075t35r3500000m1p1.5MD and p075t35r3500000m1p1.5FD

Figure 2 demonstrates that this is not an isolated case but a part of a wider hysteresis transition.

Figure 2: Hysteresis phenomenon in the ratio $\widetilde{M}_p^{\text{dip}}/\overline{M}_p^{\text{dip}}$ as a function of τ in the case $P = 0.75$, $P_m = 1.5$, $R = 3.5 \times 10^6$.

4. Comparison of the two attractors

4.1. Time dependence

Typically, MD dynamos are non-oscillatory while the FD dynamos are oscillatory. This is illustrated in the following figures.

Figure 3: Contour plots of B_φ , B_r averaged in time (left) and for a typical moment $t =$ (right) in a MD dynamo. at parameter values identical to the case in figure 3.

Figure 4: A period of dipolar dynamo oscillations of a FD dynamo at $P =$, $R =$, $\tau =$, $P_m =$. Contour plots of B_φ , B_r etc are shown at equidistant times. Parameter values are identical to the case in figure 3.

4.2. Spatial structures and spectra

We discuss spectral structures of the magnetic field for MD and FD dynamos. We also show latitudinal l , azimuthal m , and radial n spectra which provide information about the level of turbulence, spatial scales and numerical resolution of the solution.

Figure 5: l, m, n spectra of kinetic E , magnetic M energies and temperature perturbation Θ for a FD and a MD case.

4.3. Other quantities of interest

A lot of discussion during the program was devoted to dynamo quantities such as helicity, magnetic helicity, cross-helicity in view of their role in generating and dissipating dynamo action. In the following figures we demonstrate these quantities computed from first-principles in a self-consistent dynamo model.

Figure 6: Helicity, magnetic helicity, cross-helicity of a MD case - average and typical snapshots. — included in fig 3.

Figure 7: Helicity, magnetic helicity, cross-helicity in a period of FD oscillation. — included in fig 4.

5. Comparison of convection

The existence of distinguishable attractors is an entirely magnetic phenomenon. To demonstrate this we compare the structure of the convective flows for the two attractor types. We use the following figures.

Figure 8: Kinetic quantity ratios of a FD to a MD case. Ratios include Nu_i^{FD}/Nu_i^{MD} , E^{FD}/E^{MD} , $\overline{E}_p^{FD}/\overline{E}_p^{MD}$, $\overline{E}_p^{FD}/\overline{E}_p^{MD}$, $\overline{E}_t^{FD}/\overline{E}_t^{MD}$, $\overline{E}_t^{FD}/\overline{E}_t^{MD}$. Note: We expect that all ratios will have values near 1, and only $\overline{E}_t^{FD}/\overline{E}_t^{MD}$ will be greater than one. This can be explained by the effect of magn fields on diff rotation. Other ratios will be also weakly affected but this is an interesting question to discuss.

Figure 9: Spatial structures of convection on a **FD** a **MD** case - average and typical snapshots.

Figure 10: A period of relaxation oscillations in a the corresponding purely-convective case.

6. Width of the basins of attraction

6.1. Random initial conditions

What happens if the cases are started from random initial conditions?

Figure 11:

6.2. Initial condition is a combination of **MD** and **FD**

What happens if the cases are started from initial conditions that are a combination of **MD** and **FD**?

Let $\alpha \in [0, 1]$ is a continuation parameter. Take initial conditions in the form

$$IC = \alpha FD + (1 - \alpha) MD.$$

and vary α .

α	0	0.25	0.5	0.75	1
$\overline{M}_p/\overline{M}_p$	same	??	??	??	same
type	MD	??	??	??	FD

Table 1: Attractor type as a function of α .

7. Can a transitional dynamo change attractor spontaneously?

Take our reversal cases reported in PEPI 2009 and speculate that they are transitional.

Figure 13: The ratio $\overline{M}_p/\overline{M}_p$ determining the attractor type as a function of time for a typical reversal case.

Note: I expect to observe that the case is mostly **MD** with occasional excursions to **FD**. When in **FD** state reversals occur. pc.p01t100r4500000m1p05c6hb

8. Reversals

The case p075t30r2600000m1p1.5FD exhibits aperiodic reversals. This is a case which switches between strongly FD and weaker FD dynamo.

p075t50r4300000m1p1.5FD - another case where reversals might occur.

p075t40r3500000m1p1.5FD - aperiodic reversals, continue!!!

9. Conclusion

1. We present new results on multiple nonlinear attractors obtained in a model of convection-driven dynamos in rotating spherical shells.
2. We establish the existence of a hysteresis loop with variation of the rotation parameter τ .
3. We investigate the question of the width of the basins of attraction of the possible distinguishable dynamo states and the possibility of spontaneous transition between them.
4. We propose a possible mechanism of reversals.

References

- [1] E. Dormy, J.-P. Valet, V. Courtillot, *Geochem. Geophys. Geosyst.* 1 (2000) 2000GC000062.
- [2] M. Kono, P. Roberts, *Rev. Geophys.* 40 (2002) 1013.
- [3] W. Kuang, J. Bloxham, *Nature* 389 (1997) 371.
- [4] E. Dormy, A. Soward (Eds.), *Mathematical Aspects of Natural Dynamos*, CRC Press, 2007.
- [5] F. H. Busse, *Annu. Rev. Fluid Mech.* 32 (2000) 383.
- [6] E. Grote, F. H. Busse, A. Tilgner, *Phys. Earth Planet. Inter.* 117 (2000) 259.
- [7] E. Grote, F. H. Busse, *Fluid Dyn. Res.* 28 (2001) 349.
- [8] R. Simitev, F. H. Busse, *J. Fluid Mech.* 532 (2005) 365.
- [9] F. H. Busse, R. Simitev, *Geophys. Astrophys. Fluid Dyn.* 100 (2006) 341.
- [10] A. Tilgner, *Int. J. Num. Meth. Fluids* 30 (1999) 713.
- [11] U. Christensen, P. Olson, G. Glatzmaier, *Geophys. J. Int.* 138 (1999) 393.

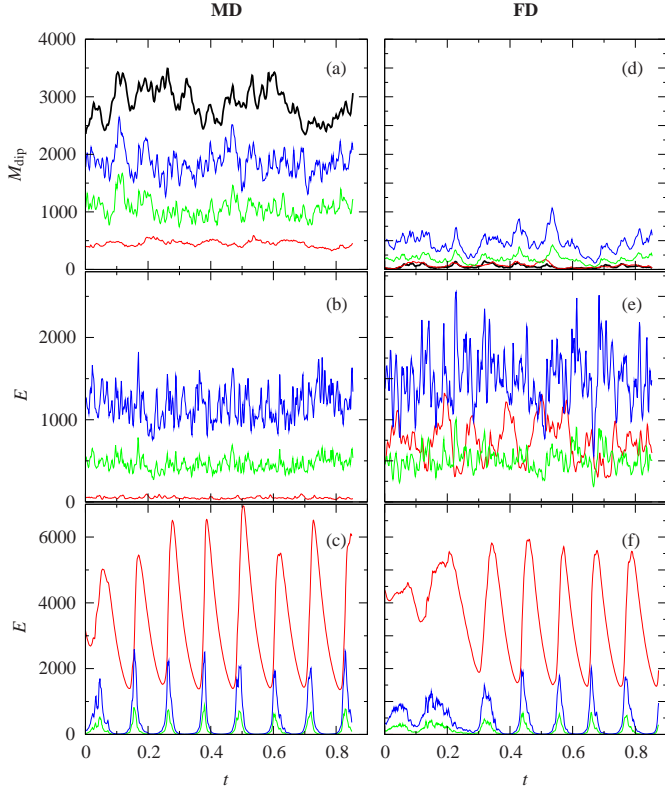


Figure 1: (Color online) Co-existing distinct chaotic attractors at identical parameter values – a **MD** (left column (a,b)) and a **FD** dynamo (right column (c,d)) both in the $R = 1.5 \times 10^6$, $\tau = 2 \times 10^4$, $P = 0.75$ and $P_m = 1.5$. The panels (a,d) show time series of magnetic energy densities. The rest of the panels show kinetic energy densities in the presence of magnetic field (b,e) and after the magnetic field is removed (c,f). The component \bar{X}_p is shown by thick solid black line, while \bar{X}_r , \bar{X}_p , and \bar{X}_t are shown by thin red, green and blue lines, respectively. X stands for either M or E .

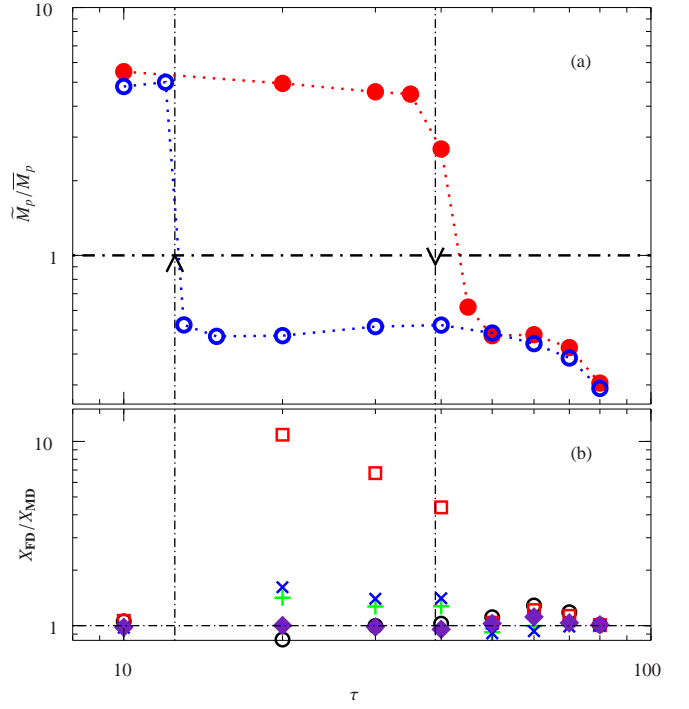


Figure 2: (Color online) (a) Co-existence and hysteresis phenomenon in the ratio \bar{M}_p/\bar{M}_p as a function of τ in the case $P = 0.75$, $P_m = 1.5$. The values of R are given by $R = (5 - 3 \cdot 10^{-5} \tau) R_c$, i.e. $R \cdot 10^{-5} = 7.6, 17, 26, 35, 43, 51, 58, 62$ at $\tau = 10^4 n$, $n = 1..8$. **FD** and **MD** dynamos are indicated by full red and empty blue circles, respectively. The expected locations of the transitions from **FD** to **MD**, and from **MD** to **FD** dynamos are represented by thin dash-dotted lines with arrows pointing down and up, respectively. (b) Ratios of

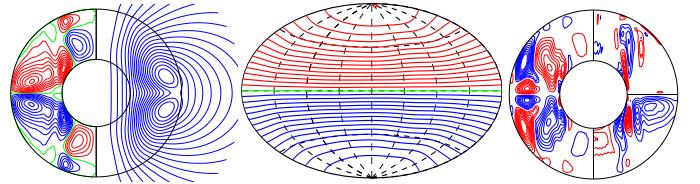


Figure 3: (Color online) Time-averaged spatial structures of a **MD** dynamo in same case as shown in Figure 1. The leftmost plot is a meridional cut showing lines of constant \bar{B}_ϕ in the left half and of $r \sin \theta \partial_\theta \bar{h}$ in the right half. The middle plot shows lines of constant B_r at $r = r_o + 1.3$. The rightmost plot is a meridional cut showing lines of constant cross-helicity XH , kinetic helicity H_u and magnetic helicity H_B at $\phi = 0$, in the left half, right upper and lower quarters, respectively.

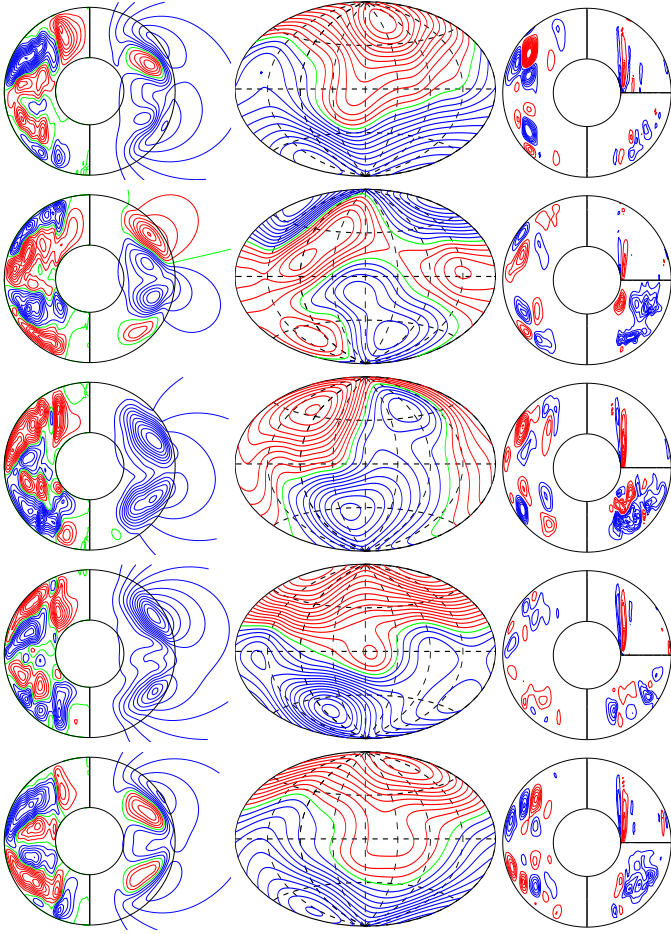


Figure 4: A period of dipolar oscillations of a **FD** dynamo in the same case as shown in Figure 1. Contour plots of the same quantities as in Figure 3 are shown at equidistant moments separated by $\Delta t = 0.0252$.

Figure 5: l, m, n spectra of kinetic E , magnetic M energies and temperature perturbation Θ for a **FD** and a **MD** case.

Figure 6: Helicity, magnetic helicity, cross-helicity of a **MD** case - average and typical snapshots.

Figure 7: Helicity, magnetic helicity, cross-helicity for a period of **FD** oscillation.

Figure 8: Kinetic quantity ratios of a **FD** to a **MD** case. Ratios include Nu_i^{FD}/Nu_i^{MD} , E^{FD}/E^{MD} , $\bar{E}_p^{FD}/\bar{E}_p^{MD}$, $\bar{E}_p^{FD}/\bar{E}_p^{MD}$, $\bar{E}_t^{FD}/\bar{E}_t^{MD}$, $\bar{E}_t^{FD}/\bar{E}_t^{MD}$.

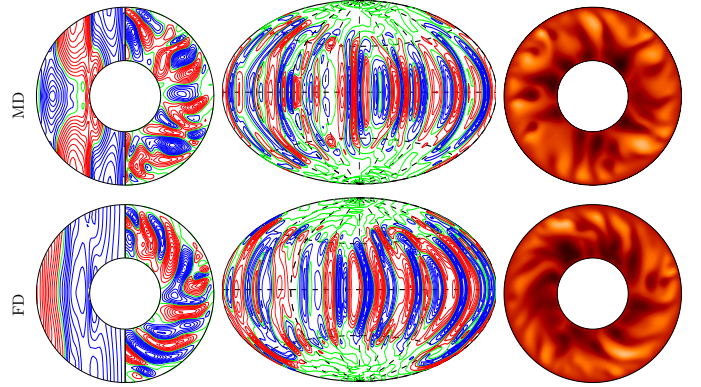


Figure 9: Spatial structures of convection in a **MD** and a **FD** with identical parameter values for the same cases shown in figure 1.

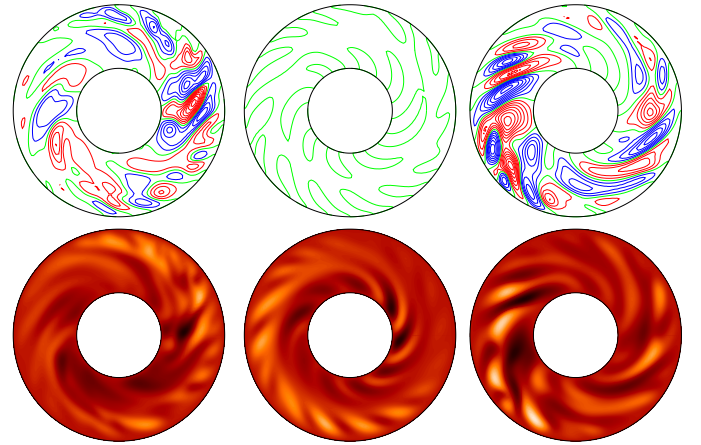


Figure 10: A period of relaxation oscillations in a purely-convective case.

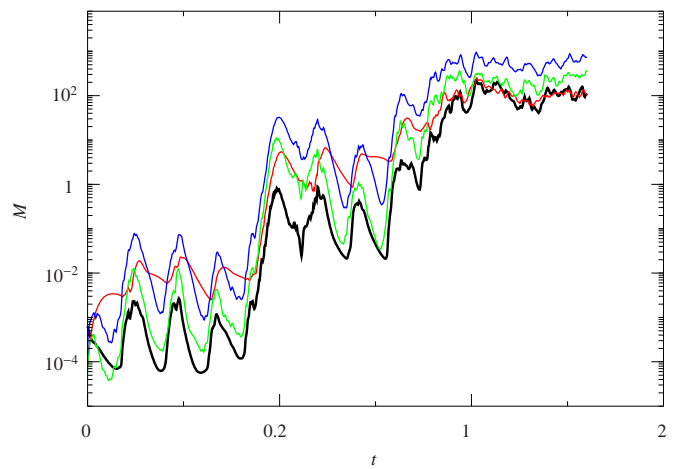


Figure 11: Infinitesimally small random magnetic field seed.

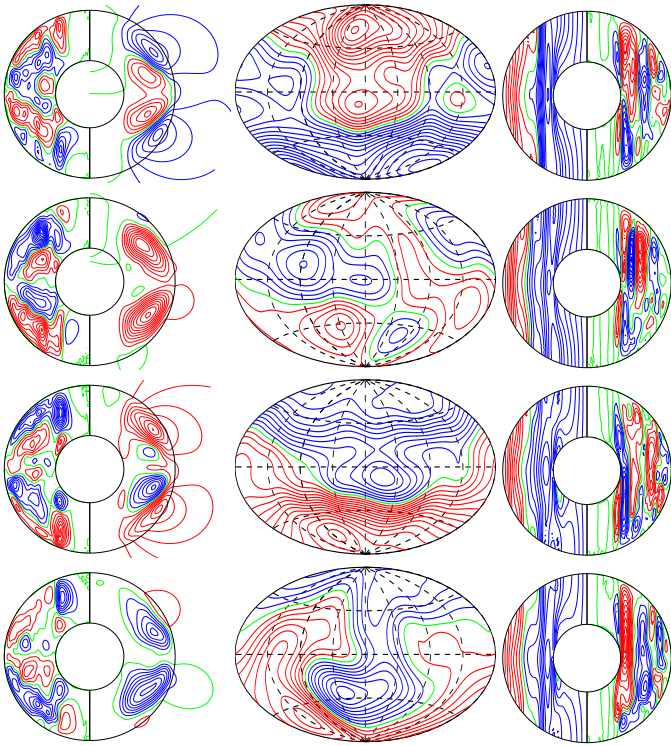


Figure 12: A periodic reversal of a **FD** dynamo in the same case as shown in Figure 1. Contour plots of the same quantities as in Figure 3 are shown at equidistant moments separated by $\Delta t = 0.0161$. The next row (not shown) is essentially the same as the first one.

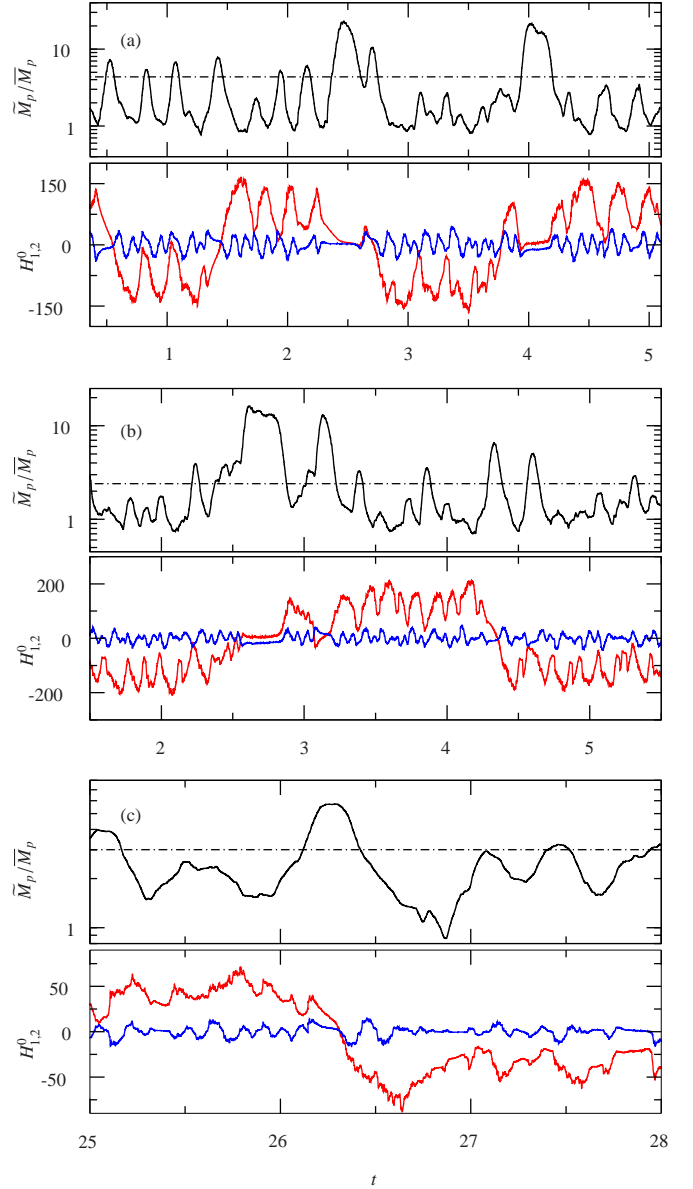


Figure 13: The ratio $\tilde{M}_p^{\text{dip}}/\overline{M}_p^{\text{dip}}$ determining the attractor type as a function of time for a typical reversal case.

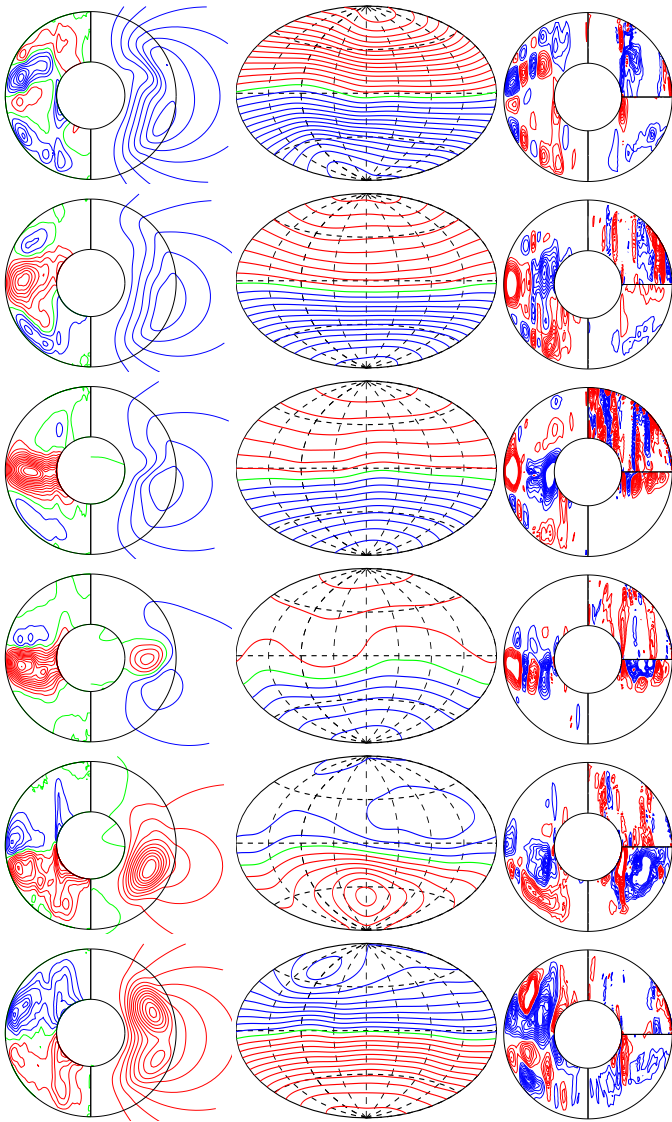


Figure 14: An aperiodic reversal in the case $pc.p01t100r4500000m1p05c6hb$.
 The time moments are $t=4.27, 4.29, 4.31, 4.35, 4.39, 4.43$.